Supporting Information

Highly Active Au/In_2O_3 Catalyst for the Reverse Water Gas Shift Reaction

Yuxue Zhao[a], Linlin Wu[a], Liangkai Xu[a], Rui Zou[a], Chang-jun Liu [*a,b]

[a] School of Chemical Engineering and Technology, Tianjin University, Tianjin 300350, China

[b] State Key Laboratory of Synthetic Biology, Tianjin University, Tianjin 30072, China

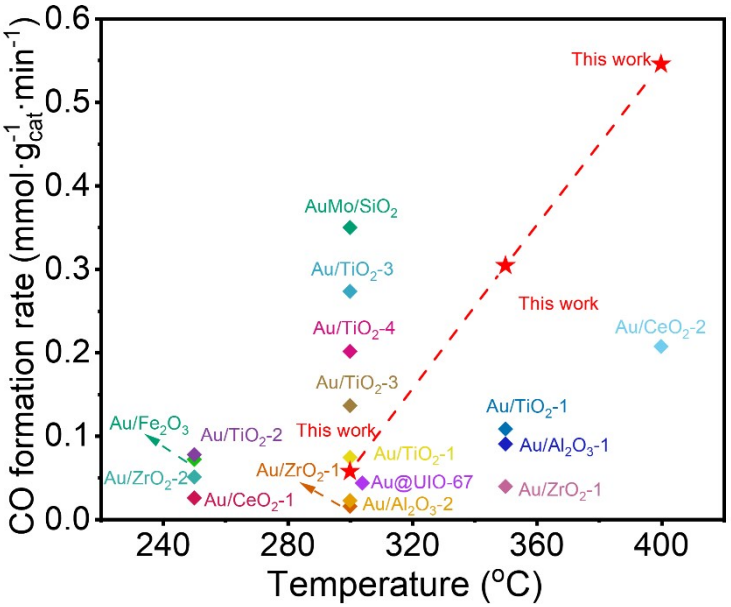

Fig. S1 RWGS catalytic activity in terms of cat-mass normalized CO formation rate of Au/In_2O_3 in comparison to Au-based catalysts reported in literature.

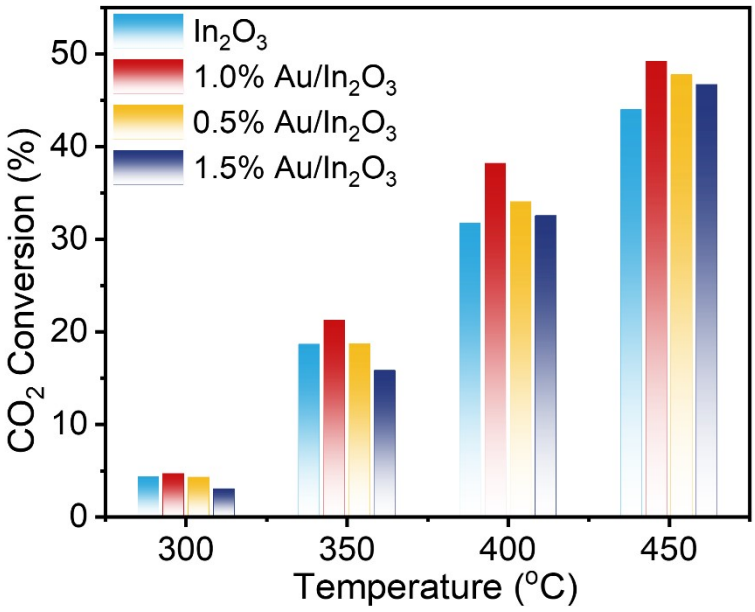

Fig. S2 Effect of Au loading on the Au/In_2O_3 catalysts.

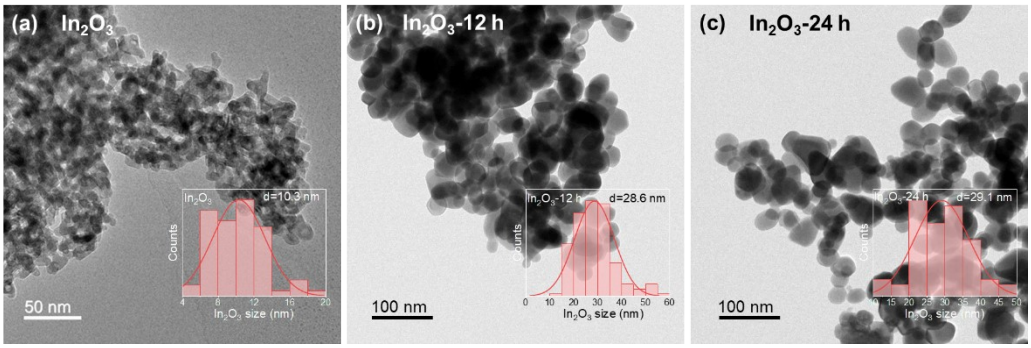

Fig. S3 TEM images of (a) In_2O_3-fresh; (b) In_2O_3-12 h; (c) In_2O_3 -24 h with In_2O_3 particle size distribution histograms.

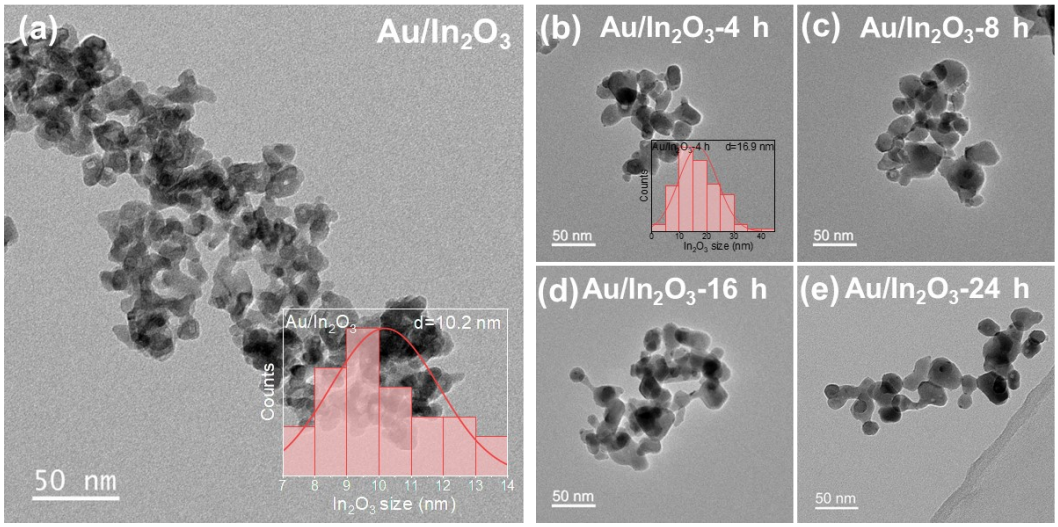

Fig. S4 TEM images of (a) Au/In_2O_3-fresh; TEM images of Au/In_2O_3 after reaction for (b) 4 h; (c) 8 h; (d) 16 h and (e) 24 h.

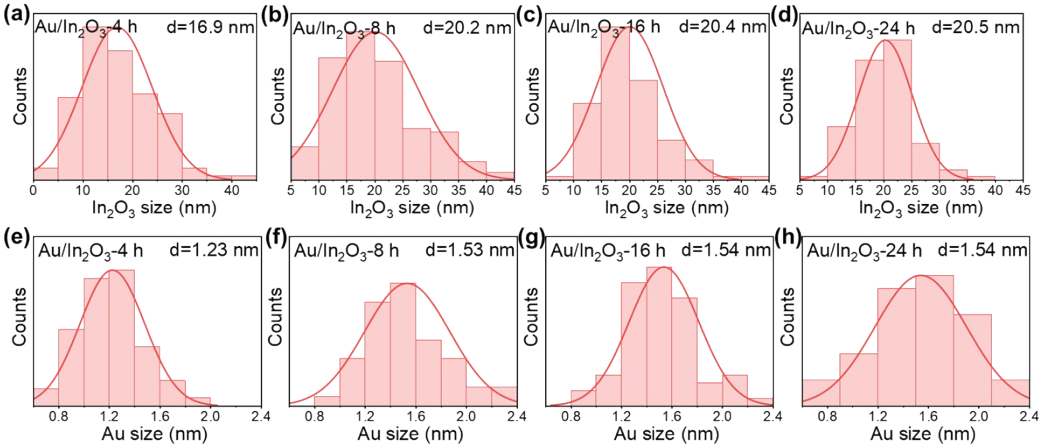

Fig. S5 The particle size distribution histograms after different reaction time of (a)-(d) Au species and (e)-(h) In_2O_3 support over Au/In_2O_3 catalyst.

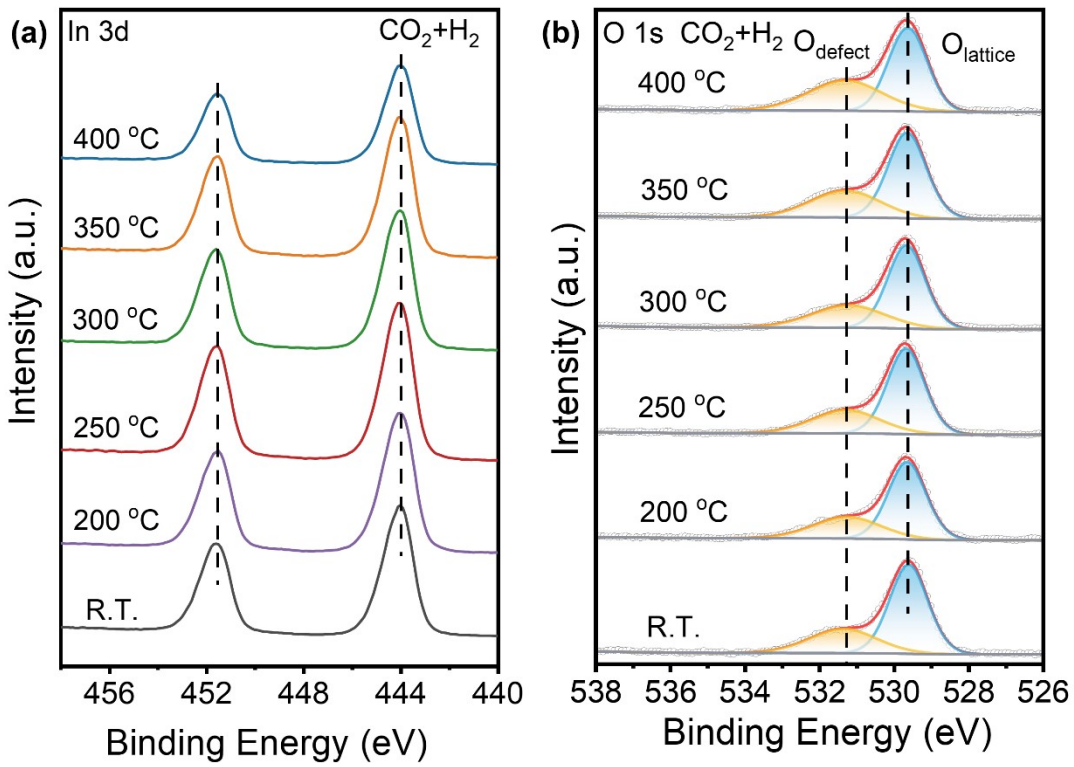

Fig. S6 *In situ* XPS spectra of (a) In 3d and (b) O 1s of the Au/In_2O_3.

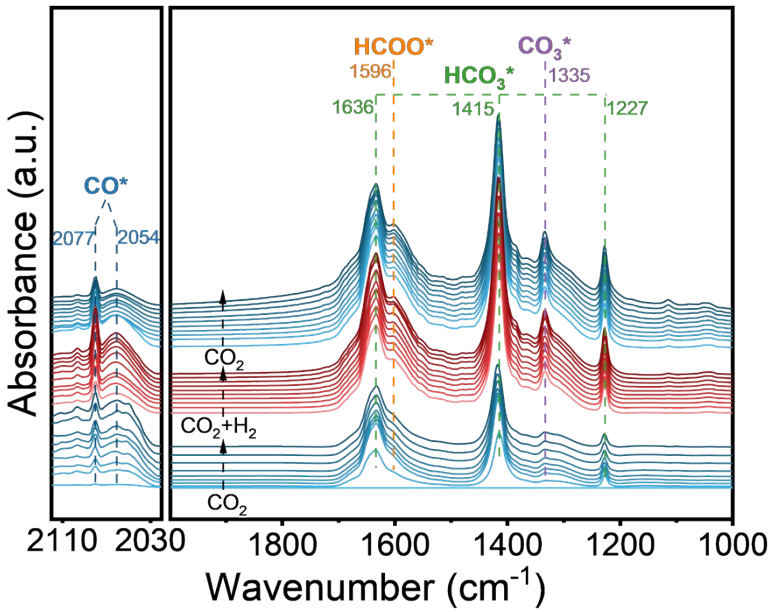

Fig. S7 The transient gas-switching *in situ* DRIFTS spectra obtained by switching gas between CO_2 and reaction gas mixture ($H_2/CO_2/N_2$ = 64/16/20) on Au/In_2O_3.

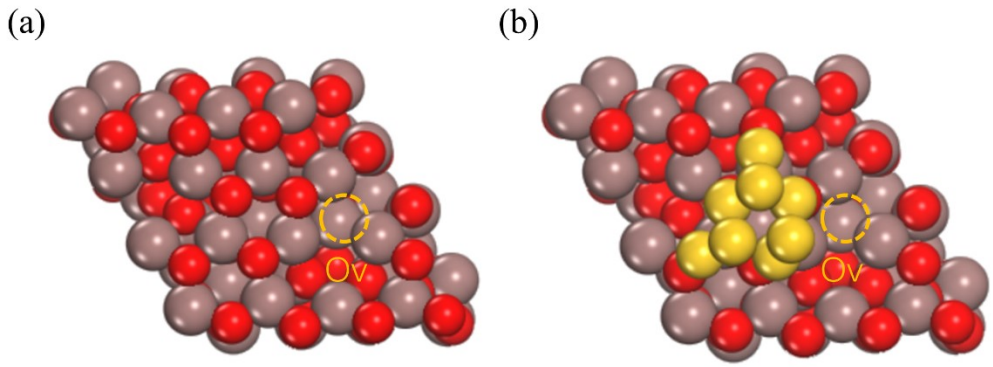

Fig. S8 Optimized configurations of (a) In_2O_3_d, (b) Au_8/In_2O_3_d.

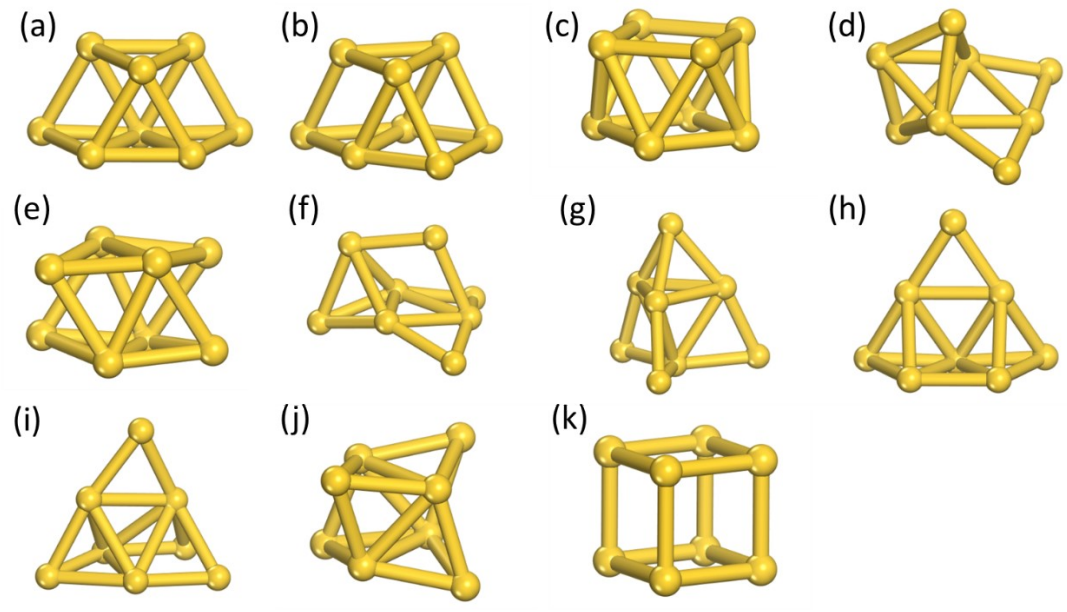

Fig. S9 (a-k) Energetically stable configurations of isolated Au_8 isomers in the gas phase.

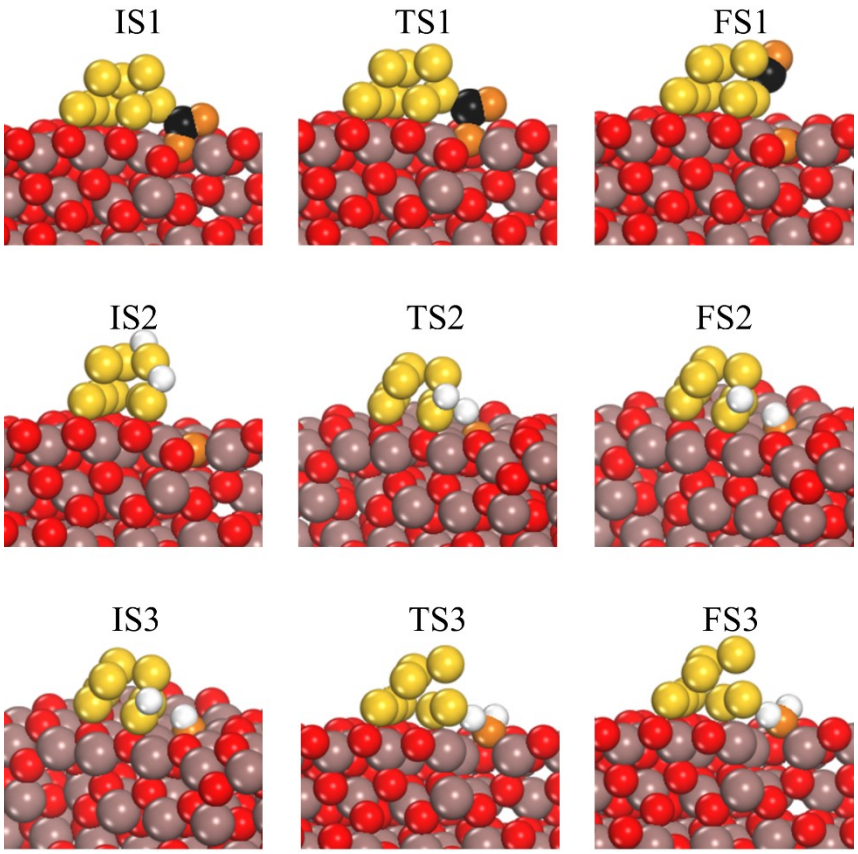

Fig. S10 Optimized configuration for each elementary step along the redox pathway over the Au_8/In_2O_3_d model. Color code: gold (yellow), indium (brown), oxygen in In_2O_3 (red), oxygen in the intermediates (orange), carbon (black), and hydrogen (white).

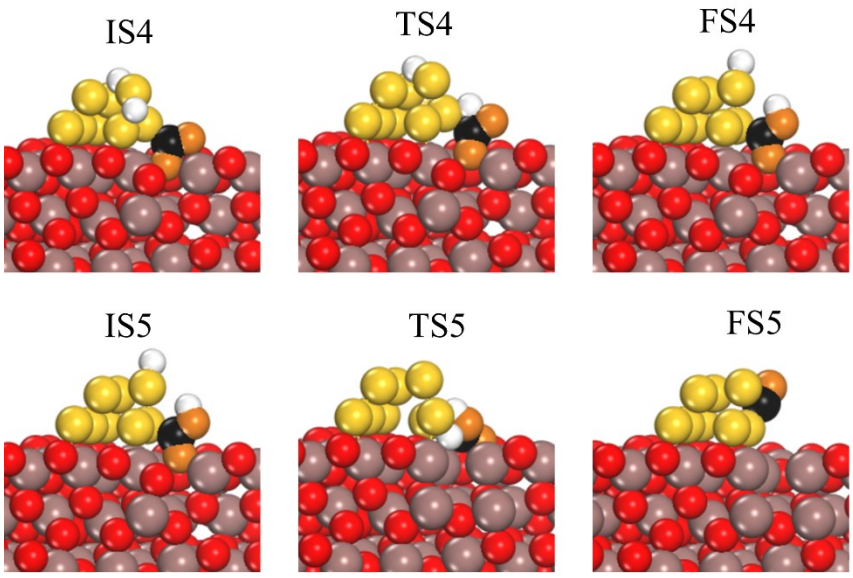

Fig. S11 Optimized configuration for each elementary step along the carboxylate pathway over the Au_8/In_2O_3_d model. Color code: gold (yellow), indium (brown), oxygen in In_2O_3 (red), oxygen in the intermediates (orange), carbon (black), and hydrogen (white).

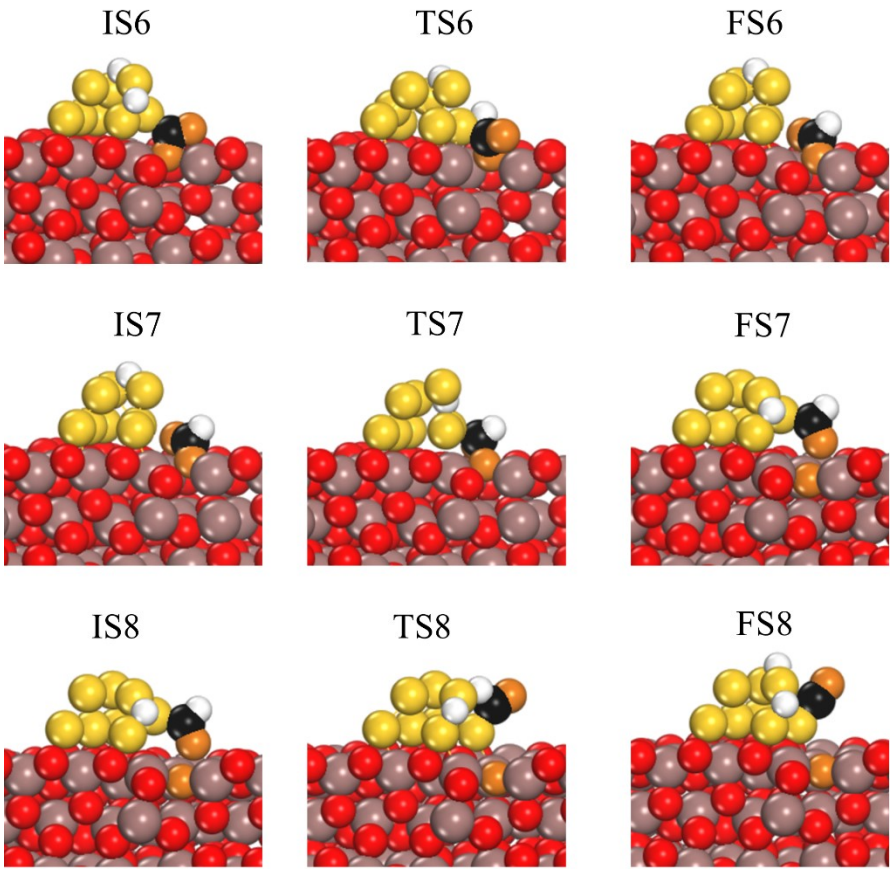

Fig. S12 Optimized configuration for each elementary step along the formate pathway over the Au_8/In_2O_3_d model. Color code: gold (yellow), indium (brown), oxygen in In_2O_3 (red), oxygen in the intermediates (orange), carbon (black), and hydrogen (white).

Table S1. Energy of Au_8 isomers in the gas phase.

Configuration	Energy (eV)	Configuration	Energy (eV)
a	-17.61	g	-17.58
b	-17.59	h	-17.51
c	-17.37	i	-17.54
d	-17.32	j	-17.53
e	-17.49	k	-17.10
f	-17.43		

Table S2. Comparison of catalytic activities in terms of cat-mass normalized CO formation rate of Au/In_2O_3 catalyst with those reported in the literature.

Catalysts	Au / wt.%	T / °C	GHSV / mL g^{-1} h^{-1}	H_2: CO_2 ratio	P / MPa	CO_2 Conv.%	CO Selec.%	CO formation rate / mmol g_{cat}^{-1} min^{-1}	Ref.
Au/TiO_2-1	0.05	350	5225	3:1	0.3	16.2	99.9	0.108	1
Au/ZrO_2-1	0.08	350	5225	3:1	0.3	5.8	99.9	0.039	1
Au@UIO-67	2.4	304	12000	3:1	2	2	96.5	0.043	2
Au/ZrO_2-2	8.4	250	3000	3:1	0.8	9.2	96.7	0.050	3
Au/Fe_2O_3	6.5	250	3000	3:1	0.8	14.7	95.2	0.072	3
Au/CeO_2-1	1.1	250	3000	3:1	0.8	5.2	94.8	0.025	3
Au/TiO_2-2	2.49	250	3000	3:1	0.8	16.1	93.2	0.077	3
Au/TiO_2-3	1	300	15000	1:1	0.1	12.2	100	0.136	4
Au/Al_2O_3-1	5	350	4000	5:1	0.1	20	100	0.090	5
Au/TiO_2-4	1	300	15000	4:1	0.1	18	100	0.201	6
Au/Al_2O_3-2	1	300	15000	4:1	0.1	2	100	0.022	6
Au/CeO_2-2	3	400	12000	1:1	-	15.4	100	0.207	7
$AuMo/SiO_2$	3.8	300	60000	2:1	0.8	-	-	0.350	8
Au/ZrO_2	0.04	350	10451	3:1	0.3	9.5	99.9	0.122	9
Au/In_2O_3	1	300	12000	4:1	0.1	4.7	100	0.067	This work
Au/In_2O_3	1	350	12000	4:1	0.1	21.3	100	0.304	This work
Au/In_2O_3	1	400	12000	4:1	0.1	38.2	100	0.546	This work

References

S1 A. I. M. Rabee, D. Zhao, S. Cisneros, C. R. Kreyenschulte, V. Kondratenko, S. Bartling, C. Kubis, E. V. Kondratenko, A. Brückner and J. Rabeah, *Appl. Catal. B*, 2023, **321**, 122083.

S2 H. Xu, Y. Li, X. Luo, Z. Xu and J. Ge, *Chem. Commun.*, 2017, **53**, 7953-7956.

S3 D. Bianchi, T. Chafik, M. Khalfallah and S. J. Teichner, *Appl. Catal. A*, 1993, **105**, 223-249.

S4 V. Kyriakou, A. Vourros, I. Garagounis, S. A. C. Carabineiro, F. J. Maldonado-Hódar, G. E. Marnellos and M. Konsolakis, *Catal. Commun.*, 2017, **98**, 52-56.

S5 N. Ishito, K. Hara, K. Nakajima and A. Fukuoka, *J. Energy Chem.*, 2016, **25**, 306-310.

S6 L. F. Bobadilla, J. L. Santos, S. Ivanova, J. A. Odriozola and A. Urakawa, *ACS Catal.*, 2018, **8**, 7455-7467.

S7 X. Zhu, X. Qu, X. Li, J. Liu, J. Liu, B. Zhu and C. Shi, *Chin. J. Catal.*, 2016, **37**, 2053-2058.

S8 R. Carrasquillo-Flores, I. Ro, M. D. Kumbhalkar, S. Burt, C. A. Carrero, A. C. Alba-Rubio, J. T. Miller, I. Hermans, G. W. Huber and J. A. Dumesic, *J. Am. Chem. Soc.*, 2015, **137**, 10317-10325.

S9 A. I. M. Rabee, S. Cisneros, D. Zhao, C. R. Kreyenschulte, S. Bartling, V. Kondratenko, C. Kubis, E. V. Kondratenko, A. Brückner and J. Rabeah, *Appl. Catal. B*, 2024, **345**, 123685.